16

Mechanical Testing

CHAPTER PREVIEW

The concepts of stress and strain and the elastic moduli should already be familiar. Where ceramics differ from most metals and polymers is that at room temperature most of them are brittle. Flaws play a major, often dominating, role in the mechanical behavior of ceramics. As a result, obtaining properties such as elastic moduli is often more difficult than it would be for metals: preparing the sample can lead to the introduction of flaws. Stress–strain curves for ceramics are usually obtained using a bending test rather than a tensile test. We need only to make our ceramic into a rectangular block. The brittle behavior of ceramics gives them low fracture toughness, a property that can most conveniently be obtained from indentation testing. A key point in this chapter is that when we use ceramics in load-bearing applications we need to understand the importance of flaws and how to incorporate that into our design approach.

16.1 PHILOSOPHY

The classical view of ceramic materials is:

(a) They're brittle.
(b) Dislocations are not important because they don't move.
(c) They are polycrystalline and fracture along grain boundaries.

Once again the classical view of ceramics and many of our preconceived ideas of how they behave are not always correct.

- We can bend a sheet of silicon into a tube.
- We can bend an alumina fiber into a circle.
- Dislocations move ahead of crack tips, are present at heterojunctions, and can be produced in large numbers during single crystal growth.
- Single crystal ceramics also fracture. (Figure 16.1 shows an Nd-doped YAG single crystal boule that fractured during growth).

Therefore, the modern view of ceramics is very different because:

(a) We may be using the ceramic as a thin film where stresses may be very high.
(b) Deformation at high temperatures may be important.
(c) In some special "new" ceramics, displacive transformations become important.

It is important to keep these ideas in mind when you read older texts. We are not going to provide a treatise on mechanical properties of ceramics. There are many existing books that do, and some of them are listed at the end of the chapter. What we do is look at what is special for ceramics.

The general need is to understand the response of a material to an applied stress. The stress may be applied externally or be induced by altering other parameters such as temperature (which can cause a phase transformation). The fundamental idea is the link to bonding. In Chapter 4, we described how the Young's modulus is related directly to the bond–energy curve. In Chapter 12, we described the nature of dislocations in ceramics.

The following three chapters have three special themes.

- Mechanical testing—how to do it plus the fundamentals of elastic constants, etc.
- Plastic deformation and how it is accommodated.
- Fracture and how to control it.

The starting point for most discussions of mechanical properties of materials begins with a stress–strain ($\sigma-\varepsilon$) curve for a material in tension. Figure 16.2 shows $\sigma-\varepsilon$ curves for three different materials at room temperature.

Material I: has high Young's modulus, high failure stress, low ductility, low toughness, and fractures without significant plastic deformation. *This behavior is characteristic of many ceramics.*
Material II: has moderate strength, moderate ductility, deforms plastically prior to failure, and is the toughest

C.B. Carter and M.G. Norton, *Ceramic Materials: Science and Engineering*,
DOI 10.1007/978-1-4614-3523-5_16,

FIGURE 16.1. Cracking in an Nd-doped YAG boule.

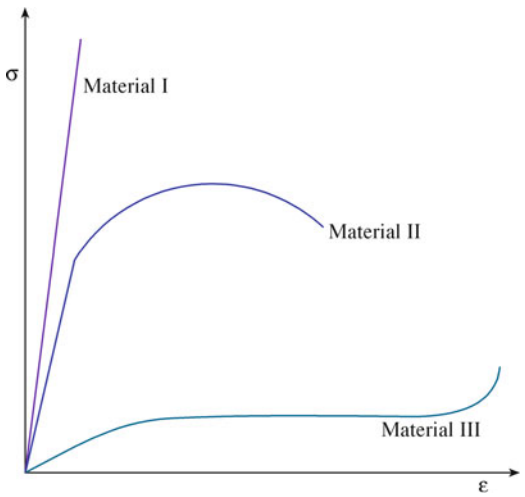

FIGURE 16.2. Idealized stress–strain curves for different materials classes.

of the three. *This behavior is characteristic of many metals.*

Material III: has low Young's modulus, is very ductile, has low ultimate tensile strength, and limited toughness. *This behavior is characteristic of many elastomers.*

The strength of ceramics is affected by many factors, and this complexity is illustrated in Figure 16.3. The composition and microstructure are particularly significant, and mechanical properties depend strongly on these characteristics. Figure 16.4 shows two specific examples that illustrate the role of microstructure on the strength

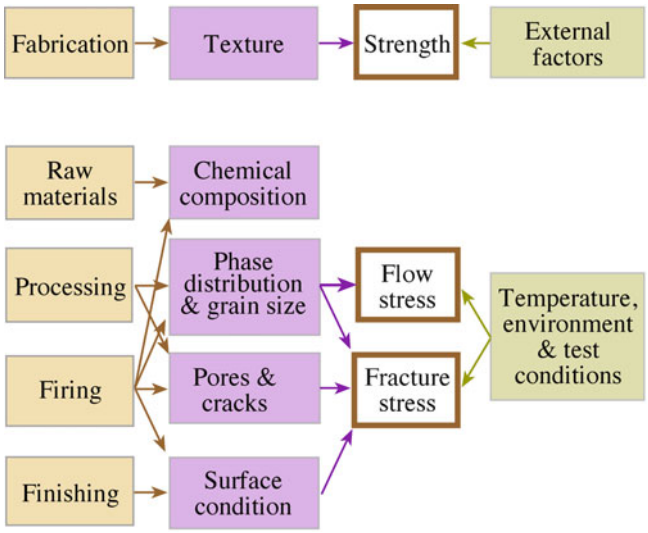

FIGURE 16.3. Factors affecting the mechanical properties of ceramics.

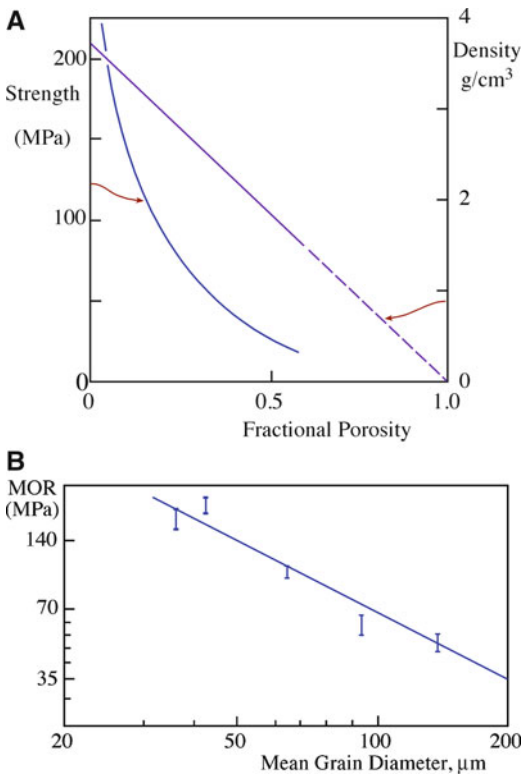

FIGURE 16.4. (A) Effect of porosity on the strength of polycrystalline Al_2O_3. (B) Effect of grain size on the strength of BeO.

of ceramics. In Figure 16.4A, the strength of a porous polycrystalline alumina is shown to decrease much more rapidly than its density. The reason is that pores act to concentrate stress, which is not uniform throughout the ceramic. The strength of nonporous ceramics decreases with increasing grain size, as illustrated for the case of BeO in Figure 16.4B. Again, the observed behavior is due to flaws in the material that act as stress concentrators. In large grains, there can be larger flaws. The effect of

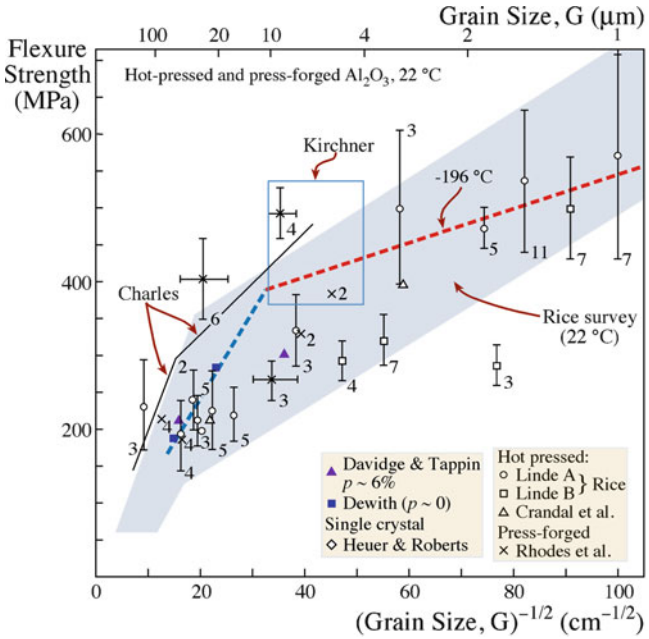

FIGURE 16.5. Compilation of strength data as a function of grain size for polycrystalline Al_2O_3.

grain size is often more complicated than that shown in Figure 16.4B when we consider ceramics where the grain size is just a few microns. Figure 16.5 is a compilation of flexural strength results for polycrystalline alumina at room temperature as a function of grain size. Despite the considerable scatter in the data, there are clearly two distinct regions. In both cases, strength is proportional to the reciprocal square root of the grain size ($d^{-1/2}$) with different constants of proportionality. The reason for this behavior is that in addition to the preexisting flaws causing brittle fracture there is a competing fracture mechanism that links dislocations and crack nucleation to subsequent failure.

It is therefore essential that when the mechanical properties of a ceramic material are listed that some details of the microstructure are also provided. As you can see from Figure 16.3, the measured value of a mechanical property may be affected by the test method. This is particularly true in the case of hardness.

High-performance structural ceramics combine the traditional advantages of ceramics (chemical inertness, high-temperature capabilities, hardness) with the ability to carry a significant tensile stress. The majority of the high-performance ceramics are based on silicon nitride, silicon carbide, zirconia, or alumina. Structural ceramics come in many forms: monoliths, composites, coatings, fibers, whiskers.

16.2 TYPES OF TESTING

Ideally, before we use a ceramic in a load-bearing application we would like to have the following information about it.

- Young's modulus
- Average strength and Weibull modulus
- Toughness
- Crack propagation rate
- Cyclic fatigue resistance
- Creep curves
- Stress rupture data

We would also like to know these parameters as a function of temperature, in particular over the temperature range at which our ceramic component is going to be used. Many different types of test are used to obtain the mechanical properties of ceramics. There are big differences between how metals are tested compared to ceramics.

- It is often difficult to do tension tests on ceramics because of the possibility of introducing flaws.
- Ceramics are stronger in compression than they are in tension because of how cracks propagate.
- For ceramics, we need to be concerned with statistics because we don't know where the largest flaws are.

Because some mechanical properties depend on how the material was tested, it is important and necessary to establish specified test methods. Standard test methods have been adopted for ceramics. In the United States, ASTM International (originally the American Society for Testing and Materials, or ASTM) is the primary organization developing standards for materials testing. ASTM Committee C-28 on Advanced Ceramics has completed several standards. Those related to mechanical properties and testing are listed in Table 16.1. Specialized subcommittees work on specific areas within the field of advanced ceramics. Committee C28.01 is involved with standards related to mechanical properties and performance of monolithic ceramics. Committee C28.02 deals with reliability issues. The National Institute of Standards and Technology (NIST) has established several free databases that list mechanical properties of ceramics.

16.3 ELASTIC CONSTANTS AND OTHER "CONSTANTS"

In this section we define some of the parameters that describe the mechanical behavior of materials. Some of these parameters are constants, such as Young's modulus $\mathcal{E}$. Some, such as hardness, are not. Hardness depends on how the material was tested.

Table 16.2 lists four elastic constants for different ceramics. These are the four that you will find crop up most commonly.

1. $\boldsymbol{\mathcal{E}}$ (or $\boldsymbol{Y}$, but be careful because $\boldsymbol{Y}$ is also used in our expression for stress intensity factor)—Young's modulus (also referred to as the elastic modulus) is a

TABLE 16.1 ASTM Standards on Mechanical Properties and Testing of Ceramics

Ceramic	*Mechanical properties and performance*
C1161-02 (2008)	Test method for flexural strength of advanced ceramics at ambient temperature[a]
C1198-09	Test method for dynamic Young's modulus, shear modulus, and Poisson's ratio for advanced ceramics by sonic resonance
C1211-02 (2008)	Test method for flexural strength of advanced ceramics at elevated temperatures
C1239-07	Standard practice for reporting uniaxial strength data and estimating Weibull distribution parameters for advanced ceramics
C1259-08	Test method for dynamic Young's modulus, shear modulus, and Poisson's ratio for advanced ceramics by impulse excitation of vibration
C1273-05 (2010)	Test method for tensile strength of monolithic advanced ceramics at ambient temperature
C1291-00 (2010)	Test method for elevated temperature tensile creep strain, creep strain rate, and creep time-to-failure for advanced monolithic ceramics
C1322-05 (2010)	Standard practice for fractography and characterization of fracture origins in advanced ceramics
C1326-08	Test method for Knoop indentation hardness of advanced ceramics
C1327-08	Test method for Vickers indentation hardness of advanced ceramics
C1361-10	Practice for constant-amplitude, axial, tension-tension cyclic fatigue of advanced ceramics at ambient temperature
C1366-04 (2009)	Test method for tensile strength of monolithic advanced ceramics at elevated temperatures
C1368-10	Test method for determination of slow crack growth parameters of advanced ceramics by constant stress-rate flexural testing at ambient temperature
C1421-10	Test method for the determination of fracture toughness of advanced ceramics
C1424-10	Test method for compressive strength of monolithic advanced ceramics at ambient temperatures
C1465-08	Test method for determination of slow crack growth parameters of advanced ceramics by constant stress-rate flexural testing at elevated temperature
C1495-07	Standard test method for effect of surface grinding on flexure strength of advanced ceramics
C1499-09	Test method for monotonic equibiaxial flexural strength testing of advanced ceramics at ambient temperature
C1525-04 (2009)	Standard test method for determination of thermal shock resistance for advanced ceramics by water quenching
C1576-05 (2010)	Standard test method for determination of slow crack growth parameters of advanced ceramics by constant stress flexural testing (stress rupture) at ambient temperature
C1683-10	Standard practice for size scaling of tensile strengths using Weibull statistics for advanced ceramics
C1684-08	Standard test method for flexural strength of advanced ceramics at ambient temperature-cylindrical rod strength
	Reliability
C1175-99 (2010)	Standard guide to test methods for nondestructive testing of advanced ceramics
C1212-98 (2010)	Standard practice of fabricating ceramic reference specimens containing seeded voids
C1239-07	Standard practice for reporting uniaxial strength data and estimating Weibull distribution parameters for advanced ceramics
C1322-05 (2010)	Standard practice for fractography and characterization of fracture origins in advanced ceramics
C1336-96 (2008)	Standard practice for fabricating nonoxide ceramic reference specimens containing seeded inclusions
C1495-07	Standard test method for effect of surface grinding on flexure strength of advanced ceramics

[a]Standards for both three-point and four-point bending, -XX: year of current version of standard, e.g., −10 is 2010

material constant defined by equation 16.1 for a linear elastic material under uniaxial tensile or compressive stress.

$$\sigma = \mathcal{E}\varepsilon \tag{16.1}$$

It is therefore the slope of a $\sigma-\varepsilon$ curve where only elastic deformation occurs.

2. $\boldsymbol{\nu}$—Poisson's ratio is the negative ratio of the transverse strain (ε_T) to longitudinal strain (ε_L).

$$\nu = -\varepsilon_T/\varepsilon_L \tag{16.2}$$

For many ceramics and glasses it is in the range 0.18–0.30.

3. $\boldsymbol{\mu}$—Shear modulus is the ratio of shear stress to shear strain.

$$\mu = \tau/\gamma \tag{16.3}$$

4. $\boldsymbol{B}$—Bulk modulus is the ratio of stress to strain for hydrostatic compression.

$$B = -P(\Delta V/V) \tag{16.4}$$

Although these constants are related directly to bonding forces between atoms, in real ceramics they are affected by microstructure (e.g., porosity and the presence of second phases). Because strain is dimensionless, elastic moduli have the same dimensions as those of stress: force per unit area (N/m^2) or, in the SI classification, Pa.

Some texts use a pair of related elastic constants $\boldsymbol{\lambda}$ and $\boldsymbol{\mu}$. These are known as the Lamé constants. We already defined μ, so it is only λ that is new. The expressions that relate elastic moduli are given in Table 16.3.

$\boldsymbol{K_I}$—Stress intensity factor is a combination of flaw size, c, and applied stress, σ.

$$K_I = \sigma Y\sqrt{c} \tag{16.5}$$

TABLE 16.2 Elastic Constants of Selected Polycrystalline Ceramics (20°C)

Material	*Crystal type*	μ *(GPa)*	B *(GPa)*	ν	$\mathcal{E}$ *(GPa)*
Carbides					
C	Cubic	468	416	0.092	1,022
SiC	Cubic	170	210	0.181	402
TaC	Cubic	118	217	0.270	300
TiC	Cubic	182	242	0.199	437
ZrC	Cubic	170	223	0.196	407
Oxides					
Al_2O_3	Trigonal	163	251	0.233	402
Al_2O_3·MgO	Cubic	107	195	0.268	271
BaO·TiO_2	Tetragonal	67	177	0.332	178
BeO	Tetragonal	165	224	0.204	397
CoO	Cubic	70	185	0.332	186
FeO·Fe_2O_3	Cubic	91	162	0.263	230
Fe_2O_3	Trigonal	93	98	0.140	212
MgO	Cubic	128	154	0.175	300
2MgO·SiO_2	Orthorhombic	81	128	0.239	201
MnO	Cubic	66	154	0.313	173
SrO	Cubic	59	82	0.210	143
SrO·TiO_2	Cubic	266	183	0.010	538
TiO_2	Tetragonal	113	206	0.268	287
UO_2	Cubic	87	212	0.319	230
ZnO	Hexagonal	45	143	0.358	122
ZrO_2-12Y_2O_3	Cubic	89	204	0.310	233
SiO_2	Trigonal	44	38	0.082	95
Chalcogenides					
CdS	Hexagonal	15	59	0.38	42
PbS	Cubic	33	62	0.27	84
ZnS	Cubic	33	78	0.31	87
PbTe	Cubic	22	41	0.27	56
Fluorides					
BaF_2	Cubic	25	57	0.31	65
CaF_2	Cubic	42	88	0.29	108
SrF_2	Cubic	35	70	0.29	90
LiF	Cubic	48	67	0.21	116
NaF	Cubic	31	49	0.24	77
Other halides					
CsBr	Cubic	8.8	16	0.26	23
CsCl	Cubic	10	18	0.27	25
CsI	Cubic	7.1	13	0.27	18
KCl	Cubic	10	18	0.27	25
NaBr	Cubic	11	19	0.26	28
NaCl	Cubic	15	25	0.25	38
NaI	Cubic	8.5	15	0.27	20
RbCl	Cubic	7.5	16	0.29	21

All values were calculated from single-crystal data

Y in equation 16.5 is a dimensionless parameter that depends on the crack and loading geometries. For a simple interior crack of length $2c$ and tensile loading, $Y = \sqrt{\pi}$ (this is the original geometry considered by Griffith); for a surface crack under similar loading, $Y = \sqrt{(\pi/2)}$. The units of K_I are MPa.m$^{1/2}$.

The subscript refers to the type of loading geometry. There are three fundamental deformation modes that can be important for crack propagation. These modes are illustrated in Figure 16.6.

- Mode 1 opening. The most important for crack propagation in brittle solids. Can be achieved by an applied uniaxial tension
- Mode 2 sliding
- Mode 3 tearing

K_{Ic}—Critical stress intensity factor or fracture toughness. Fracture of a material in tension occurs when $K_I \geq K_{Ic}$.

H—Hardness. There are different types of hardness. Why? Because the value of a material's hardness depends on how it is tested. The hardness of a material is its resistance to the formation of a permanent surface impression by an indenter. You also see it defined as resistance of a material to deformation, scratching, and erosion. Hence, the geometry of the indenter tip and the crystal orientation (and therefore the microstructure) affect the hardness. In ceramics, there tends to be wide variations in hardness because it involves plastic deformation and cracking. Table 16.4 lists hardness values on the Mohs' hardness scale, a scratch test that can be used to compare hardness of

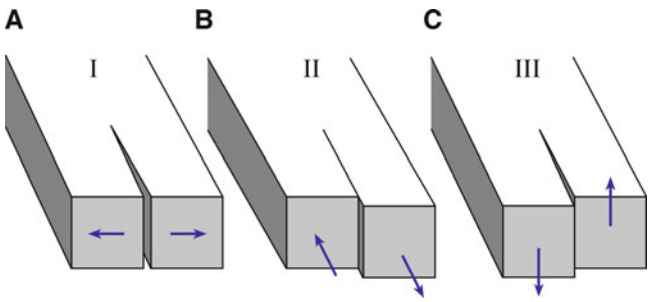

FIGURE 16.6. The three deformation modes for fracture: (A) Mode I opening. (B) Mode II sliding (in-plane shearing). (C) Mode III tearing (anti-plane shearing).

TABLE 16.3 Expressions for Various Isotropic Elastic Moduli; Various Pairs of Moduli

	Independent Pairs of Moduli			
Moduli	$\mathcal{E}$, μ	B, μ	B, ν	λ, μ
$\mathcal{E}$	$\mathcal{E}$	$9B\,\mu/(3B+\mu)$	$3B(1-2\nu)$	$\mu(3\lambda+2\,\mu)/(\lambda+\mu)$
μ	μ	μ	$3B(1-2\nu)/2(1+\nu)$	μ
B	$\mathcal{E}\mu/3(3\mu-\mathcal{E})$	B	B	$\lambda+(2\,\mu/3)$
ν	$(\mathcal{E}/2\mu)-1$	$(3B-2\,\mu)/(6B+2\,\mu)$	ν	$\lambda/(2\lambda+\mu)$
λ	$(\mathcal{E}-2\mu)\mu/3(3\mu-\mathcal{E})$	$B-(2\,\mu/3)$	$3\nu B(1+\nu)$	λ

TABLE 16.4 Mohs' Hardness

Hardness no.	*Mohs'scale*	*Ridgeway's extension of Mohs' scale*	*Knoop hardness expanded scale*
1	Talc	Talc	
2	Gypsum	Gypsum	32
3	Calcite	Calcite	135
4	Fluorite	Fluorite	163
5	Apatite	Apatite	430
6	Orthoclase	Orthoclase	560
7	Quartz	Vitreous silica	—
8	Topaz	Quartz or stellite	820
9	Corundum	Topaz	1,340
10	Diamond	Garnet	1,360
11		Fused zirconia	—
12		Fused alumina	2,100
13		Silicon carbide	2,480
14		Boron carbide	2,750
15		Diamond	7,000

different minerals. For example, quartz has a Mohs' hardness of 7, which made flint (a cryptocrystalline quartz) particularly useful in prehistoric times for shaping bone (mineral component is apatite: hardness of 5) and shell (mineral component is calcite: hardness of 3). Mohs' was not the first scratch hardness technique. As long ago as 1690, Christian Huygens, the famous astronomer, had noticed anisotropy in scratch hardness.

Brittleness—Although not widely used, the brittleness index (BI) has been used to quantify the brittleness of a ceramic, where $\text{BI} = H/K_{\text{Ic}}$.

16.4 EFFECT OF MICROSTRUCTURE ON ELASTIC MODULI

In Chapter 4, we showed that Young's modulus is a property that is directly related to the bonding forces between atoms. We also showed that it varies as a function of temperature. In real ceramics, we have to consider the fact that we often have more than one phase present. The overall modulus is then going to be a combination of the properties of each of the phases and lie somewhere between the high- and low-modulus components.

Two analytical expressions represent the upper and lower bounds for Young's modulus.

16.4.1 Voigt Model

Assumption: strain in each constituent is the same. Represents upper bound of Young's modulus.

$$\mathcal{E} = V_2\mathcal{E}_2 + (1 - V_2)\mathcal{E}_1 \tag{16.6}$$

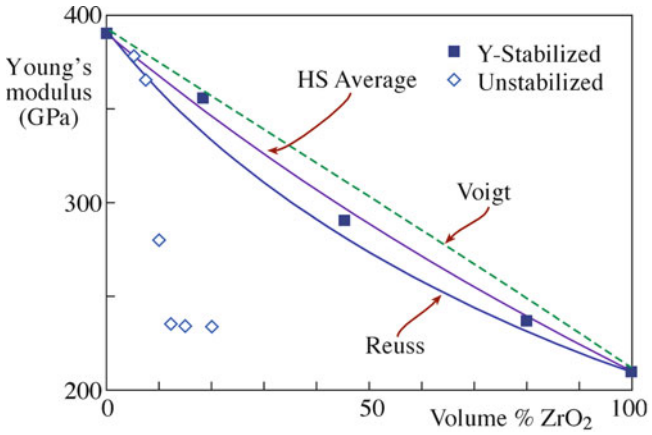

FIGURE 16.7. Comparison of predicted values of Young's modulus for an Al_2O_3-tetragonally stabilized ZrO_2 composite with experimental data.

16.4.2 Reuss Model

Assumption: Stress in each phase is the same. Represents lower bound of Young's modulus.

$$\frac{1}{\mathcal{E}} = \frac{V_2}{\mathcal{E}_2} - \frac{(1 - V_2)}{\mathcal{E}_1} \tag{16.7}$$

Hashin and Shtrikman (HS) developed a narrower, more useful, set of bounds using basic elasticity energy theorems. The HS bounds have been shown to be best for the bulk modulus and are given by:

$$\frac{B - B_1}{B_2 - B_1} = V_2\left[\frac{V_1(B_2 - B_1)}{B_1 + H}\right]^{-1} \tag{16.8}$$

where $H = 4\ \mu_2/3$ or $H = 4\ \mu_1/3$. Young's moduli can be obtained from B if ν is known and reasonable fits with experimental data can be obtained, as shown in Figure 16.7 for alumina–tetragonally stabilized zirconia (Al_2O_3–ZrO_2) composites.

If the second phase is porosity, as is often the case in polycrystalline ceramics, then intuitively we realize that there is a decrease in the elastic modulus. A pore has zero stiffness. Several relationships have been developed to account for the change in Young's modulus with porosity, P. They are shown in Table 16.5, where the "constants" a and b are often empirically determined; E_0 is the Young's modulus of the dense material.

16.5 TEST TEMPERATURE

Mechanical properties often show strong variations with temperature. We already considered in Chapter 4 how temperature affects Young's modulus. For some mechanical properties, the change with temperature may be more abrupt than the gradual decrease in $\mathcal{E}$ with increasing temperature. The ductile-to-brittle transition, which occurs

TABLE 16.5 Relations Between Porosity, *P*, and Young's Modulus, $\mathcal{E}$

$\mathcal{E} = \mathcal{E}_0(1 - aP)$	Linear decrease in Young's modulus with porosity when P is small $a \sim 4$
$\mathcal{E} = \mathcal{E}_0(1 - aP + bP^2)$	For a low concentration of spherical pores ($a \sim 1.9$, $b \sim 0.9$)
$\mathcal{E} = \mathcal{E}_0(1 - aP)^b$	For solid foams with very high porosity $P > 0.7$ ($a = 1$, $b = 2$)
$\mathcal{E} = \mathcal{E}_0\left[(1 - P)^2/1 + (a - 1)P\right]$	a is a shape factor with values depending on porosity: $a = 2.5$ for interconnected porosity ($1/a = 0.4$) $a = 3.3 - 1.4$ for porosity that resembles ribbons ($1/a = 0.3 - 0.7$) $a = 0.6 - 1.0$ for isolated pores ($1/a = 0.6 - 1.0$) ($1/a$ is known as the Nielson shape factor)
$\mathcal{E} = \mathcal{E}_0 \exp(-aP)$	Empirical for oxides with porosity in the range 0–40% ($a \sim 4$)

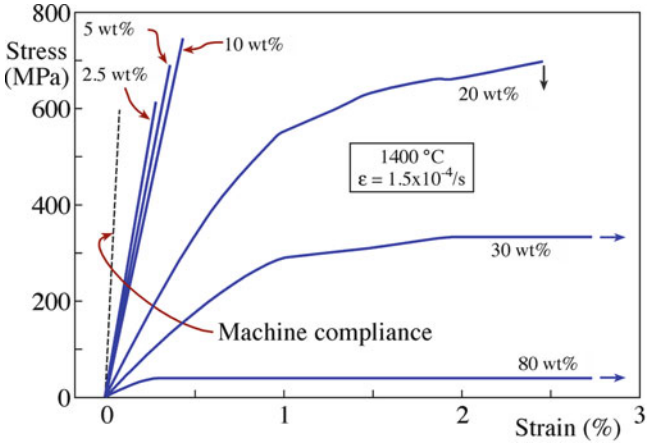

FIGURE 16.9. Stress–strain curve for Si_3N_4 at 1,400°C for various amounts of silica. The machine compliance is the inherent displacement within the instrument.

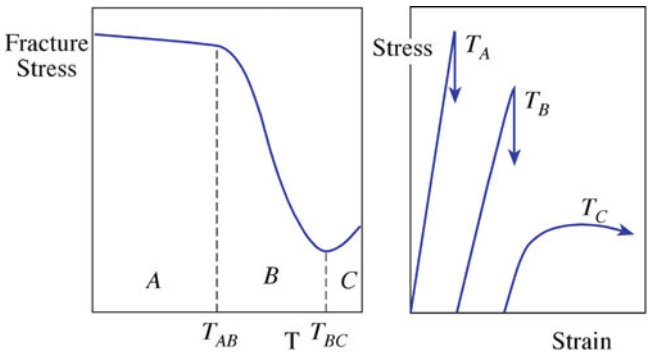

FIGURE 16.8. Effect of temperature on fracture stress for a ceramic. The key temperatures are T_{AB} and T_{BC}.

with decreasing temperature, is an important topic in metals. The significance of this phenomenon really came to light during World War II, when there were reports of serious fractures in some of the Liberty ships (mass-produced vessels of predominantly welded construction). One of the most striking instances of this type of fracture was the T2 tanker S.S. Schenectady built in Portland, Oregon, which suddenly broke into two sections at 10.30 p.m. on January 16, 1943. The reason was that the steel alloy used to construct the hull had undergone a ductile-to-brittle transition at a temperature of 4°C. This event gave particular impetus to the study of fracture in brittle materials.

Do ceramics experience a ductile-to-brittle (or the converse) transition, and is it important? Ceramics can exhibit both types of behavior over different temperature ranges. Figure 16.8 illustrates the temperature dependence of strength for ceramics.

- Region A: fracture is brittle, and the fracture strain $\sim 10^{-3}$. There is no significant plastic deformation prior to failure, and the strength varies little with temperature.
- Region B: fracture is again brittle, but slight plastic deformation occurs prior to failure. The failure strain is usually in the region of 10^{-3}–10^{-2}, and strength falls with increasing temperature.
- Region C: appreciable plastic flow occurs, with strains of the order of 10^{-1} prior to failure. This behavior is rarely observed in ceramics, even in ductile polycrystalline ceramics.

The critical temperatures, T_{AB} and T_{BC}, vary greatly for different ceramics. For polycrystalline MgO the brittle-to-ductile transition occurs at ~1,700°C (0.6 T_m). There is no plastic deformation in β-SiC below 2,000°C. Talc, MoS_2, and graphite all deform at room temperature. MoS_2 and graphite are widely used as solid lubricants.

The transition can be important in structural ceramics (particularly nonoxides such as silicon nitride) when they are used in high-temperature applications. Densification in these ceramics is often achieved using a second phase that forms a glass at grain boundaries and triple points. At temperatures near the glass-softening temperature, very extensive plastic flow occurs. Figure 16.9 shows σ−ε curves for silicon nitride at 1,400°C containing different amounts of silica. For silica contents >20 wt%, macroscopic plastic deformation occurs. At high silica contents, it is believed that the glassy phase is no longer constrained at the triple points.

16.6 TEST ENVIRONMENT

In some cases, the environment that the ceramic is exposed to is a very important consideration. For example, you often see that mechanical tests on bioceramics are performed either in vivo or in vitro. Tests performed in the body are referred to as in vivo. Tests performed outside

the body, often under conditions that seek to replicate or approximate the physiological environment, are referred to as in vitro. ISO Standard 6474 for alumina bioceramics specifies a bend strength >450 MPa after testing in Ringer's solution. Ringer's solution is a model liquid that resembles human body fluid.

RINGER'S SOLUTION (PARTS BY VOLUME)

NaCl solution 0.9%	94
KCl solution 1.15%	4
$CaCl_2$ solution 1.22%	3
KH_2PO_4 solution 2.11%	1
$MgSO_4$ solution 3.82%	1
$NaHCO_3$ solution 1.3%	14
$NaHPO_4$ solution 1 M	13

16.7 TESTING IN COMPRESSION AND TENSION

The tensile test is the most used procedure to determine the tensile strength of a metal. However, it is not used as widely for ceramics because of their inherent brittleness. It is difficult to make the typical "dog bone"-shaped samples, where the cross-sectional area is reduced in the gauge length. We could do this with a ceramic, but the machining needed to give this shape is likely to introduce surface flaws. In many tensile test instruments, the sample under test is connected by means of a screw thread. This is often tricky to machine with a ceramic, and it may also break in the grips. Finally, because ceramics fail after only about 0.1% strain, the specimens under test must be perfectly aligned; otherwise we introduce bending stresses, which complicate things.

In some practical situations, we require ceramics to support a tensile load. Consider the growth of silicon single crystals by the Czochralski process, which involves pulling the crystal from the melt. The crystal is supported entirely by a narrow region called the neck, about 3 mm in diameter. It is possible to support a total crystal weight of about 200 kg. This requirement determines the maximum overall volume of a silicon boule. The diameter is controlled by our ability to produce dislocation-free crystals, as we describe in Chapter 29. Steel reinforced concrete and safety glass are two examples of where a ceramic is prestressed in compression to increase its ability to support a tensile load.

RULE OF THUMB

Compressive fracture strength is 10–15 times greater than tensile fracture strength.

Stress–strain curves for metals look very similar and provide similar results whether the testing is carried out in tension or compression. Ceramics are generally stronger in compression and can tolerate high compressive loads. Some examples are given in Table 16.6. However, reliable compressive strength data are limited for ceramics. Note that the Young's modulus is the same because the curves have the same slope.

One ceramic that is widely tested in compression is concrete. Concrete is a ceramic–matrix composite consisting of a mixture of stone and sand (called the aggregate) in a cement matrix. The aggregate provides the strength and the cement the workability. When concrete is used in construction it must always be loaded in compression. As shown in Figure 16.10, cracks behave

TABLE 16.6 Ratio of Compressive Strength σ_{cc} to Bending Strength, σ_c

Ceramic	*Grain size (μm)*	σ_{cc}/σ_c
TiB_2	20–50	4–6
ZrB_2	20–50	4–6
B_4C	1	7
WC	1–6	4–6
Al_2O_3	1–100	4–30
$MgAl_2O_4$	1	7
ThO_2	4–60	13–17
UO_2	20–50	5–18

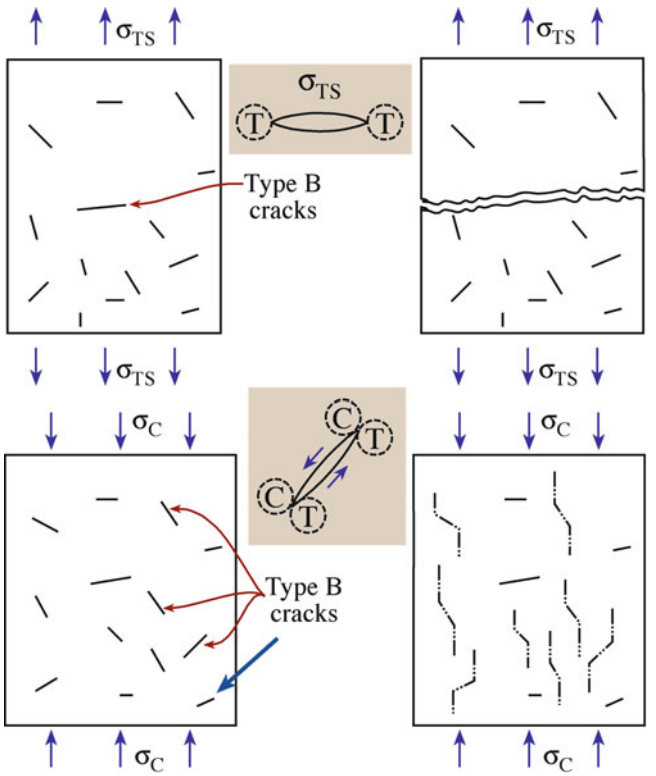

FIGURE 16.10. Unstable and stable crack propagation for a brittle material in tension (T) and compression (C), respectively. Stable crack propagation leads to crushing.

differently in compression than they do in tension. In compression, cracks twist out of their original orientation and propagate stably along the compression axis. The result is that the sample crushes rather than fractures. Fracture is not caused by rapid unstable crack propagation as it is in tension.

In tension, we are concerned with the largest crack, the "critical flaw," particularly if it is on the surface. In compression, we are concerned with the average flaw size, c_{av}. We can estimate the compressive stress to failure by substituting c_{av}, into equation 16.5 and using a multiplier between 10 and 15. Teeth are ceramic composites: they survive for years even when many cracks are present.

16.8 THREE-POINT AND FOUR-POINT BENDING

To avoid the high expense and difficulties of performing tensile tests on ceramics, tensile strength is often determined by the bend test. There are two geometries, which are illustrated in Figure 16.11. The main advantage of the bend test, other than its lower cost, is that we use simple sample geometries. The specimens have either a rectangular or cylindrical geometry. The four-point bend test is preferred because an extended region with constant bending moment exists between the inner rollers.

The maximum tensile stress in the surface of the beam when it breaks is called the modulus of rupture (MOR), σ_r. For an elastic beam, it is related to the maximum moment in the beam, M.

$$\sigma_r = \frac{6M_r}{BW^2} \tag{16.9}$$

where W is the height of the beam, and B is its thickness. For the case of bend-testing a ceramic, this equation is applicable only when the distance between the inner rollers is much greater than the specimen height.

Other terms are also used including flexural strength, fracture strength, and bend strength. The bend test is also known as a flexure test; and the resistance of a beam to bending is known as its flexural rigidity. The terminology can be a little confusing, but this test is important because it is widely used and probably the most well studied strength test for ceramics.

MODULUS OF RUPTURE EQUATIONS

3-Point Bend: $\sigma_r = \dfrac{3PL}{2BW^2}$

4-Point Bend: $\sigma_r = \dfrac{3PD}{BW^2}$

Examples of data from such tests are shown in Figure 16.12 for polycrystalline alumina. The main comment that can be made is that there is a wide variation in the values!

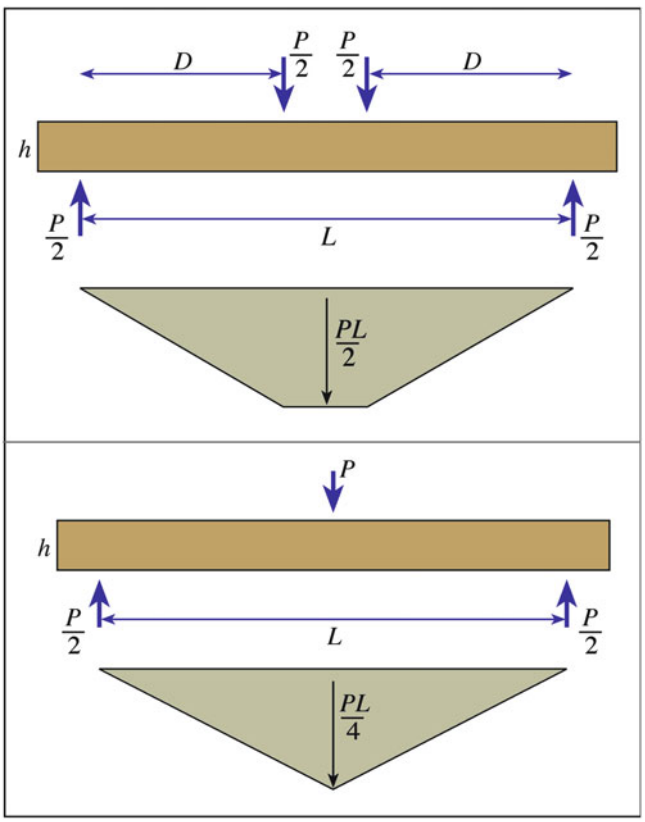

FIGURE 16.11. Geometries for three- and four-point bending.

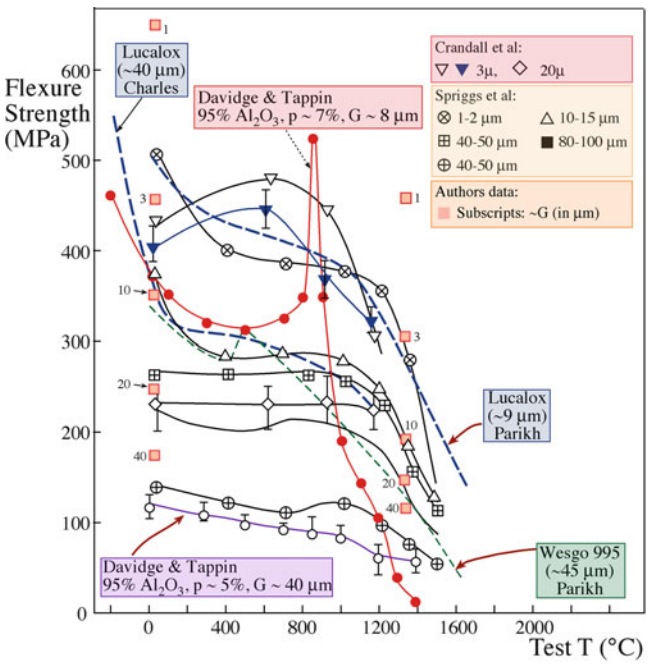

FIGURE 16.12. Flexural strength of polycrystalline Al_2O_3 as a function of test temperature.

Grain size differences between the samples clearly comprise one of the factors contributing to this variation.

The main disadvantage of the bend test is that the stress distributions can be complex and nonuniform. The consequence is that under certain conditions, particularly when the largest flaws in the sample are located in the interior of the specimen, the strength of the ceramic can be overestimated.

16.9 K_{IC} FROM BEND TEST

There are several techniques to determine K_{Ic} for a ceramic. The two main approaches are to use indentation or bending. In the bend test, a notch is introduced (usually using a diamond-tipped copper cutting wheel) into the tensile side of the specimen, as shown in Figure 16.13. In (a) the notch is flat (single-edged notched beam, SENB), in (b) it is chevron-shaped. The specimen is loaded, usually in a four-point bend, until it fails at F_{Max}, and K_{Ic} is calculated.

SENB AND CN SPECIMENS

Typical dimensions
$B = 3$ mm, $W = 4$ mm,
$S_2 = 20$ mm, $S_1 = 40$ mm
Crack depth $c/W \sim 0.5$
Total specimen length 50 mm

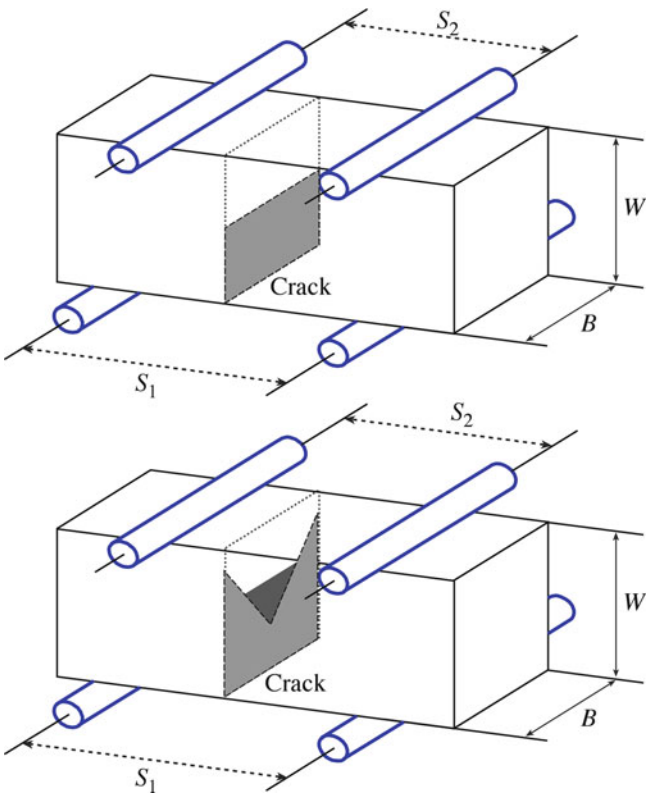

FIGURE 16.13. Geometries for single-edged notched beam (SENB) and chevron notched (CN) specimens used to determine K_{IC}.

For the SENB:

$$K_{Ic} = \frac{3\sqrt{c}(S_1 - S_2)\xi F_{Max}}{2BW^2} \qquad (16.10)$$

where c is the length of the initial crack that we introduced, and ξ is a calibration factor. The advantage of the SENB test is that it is quite simple but tends to overestimate K_{Ic} because the crack is often not atomically sharp. For ceramics with very fine grain sizes, it is necessary that the notch is very narrow.

For the chevron notched (CN) specimen

$$K_{Ic} = \frac{(S_1 - S_2)\xi^* F_{Max}}{BW^{\frac{3}{2}}} \qquad (16.11)$$

where ξ^* is a compliance function. Sometimes you see equation 16.11 written in such a way that all the geometrical terms are grouped together as a single geometric function Y^*. Then we have:

$$K_{Ic} = \frac{F_{Max}}{B\sqrt{W}} Y^* \qquad (16.12)$$

The value of Y^* is then necessary for different specimen geometries and different notch geometries. Two approaches can be used to obtain Y^*.

The advantage of the CN geometry is that we don't need to worry about introducing a sharp precrack. Our original notch is made by two saw cuts to produce a triangularly shaped cross section. A crack is easily initiated at the tip of the chevron, but the increasing cross section of the crack front causes crack growth to be stable prior to failure. Further crack extension requires an increase in the applied load, and it is possible to create an atomically sharp crack before the specimen fails. Also, you can see from equation 16.11 that we don't need to know the actual crack length. In fact, we don't need to know any of the materials' properties.

CAUTION

Fracture toughness values for different ceramics may depend on technique used to measure them.

16.10 INDENTATION

Measuring the hardness of a ceramic is important, and it is usually done using an indentation test. The basic idea is that a permanent surface impression is formed in the material by an indenter. We then measure the actual or projected area of the impression. The hardness is then determined by dividing the applied force, F, by this area. The processes that happen under the indenter tip can be

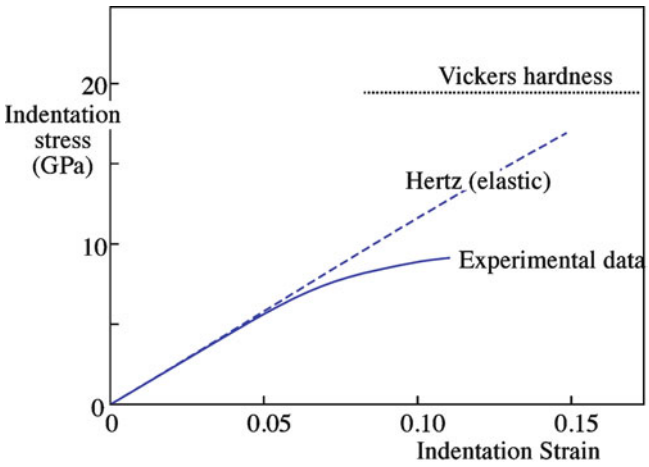

FIGURE 16.14. Indentation stress versus indentation strain.

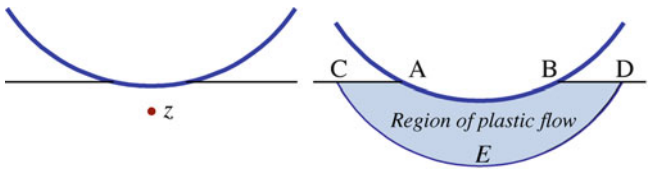

FIGURE 16.15. Plasticity under the indenter (*shaded area*) causes the deviation from Hertzian behavior.

quite complex. We often see a deviation from what is called "Hertzian" behavior, where the indentation stress is proportional to the indentation strain (Figure 16.14). The deviation is due to plasticity beneath the indenter, as illustrated in Figure 16.15. We discuss this more in Chapter 17. Cracking can also occur on indenting and can be used as a means of determining fracture toughness.

There are many different hardness tests, and each gives a different number. The common hardness tests are listed in Table 16.7, and the geometries of the impression are shown in Figure 16.16. It is possible to convert between different hardness scales, but the conversion depends on both the material and its microstructure. The most reliable data are for steels because most of the work has been done on these alloys. Detailed conversion tables for metals and

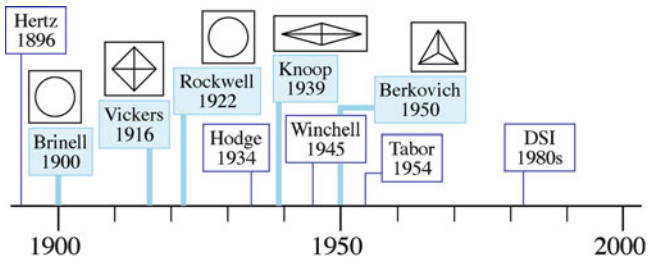

FIGURE 16.16. Evolution of common hardness tests and the corresponding indenter shapes.

alloys are available in ASTM Standard E 140, "Standard Hardness Conversion Tables for Metals." There are different regimes of hardness based on the load used, as shown in Table 16.8. These divisions are somewhat arbitrary but commonly accepted.

16.11 FRACTURE TOUGHNESS FROM INDENTATION

We can obtain the fracture toughness from indentation tests. The basic idea is illustrated in Figure 16.17. We get an indent and radial cracks. The hardness is then

$$H = P/\alpha a^2 \tag{16.13}$$

TABLE 16.8 Hardness Regimes

Regime	*Applied load (N)*	*Comments*
Microhardness	0.0098–1.96	Hardness value decreases as load increases. Possibility for very large variation in values depending on technique used and microstructure. Surface effects may dominate
Low load hardness	1.96–98.1	
Standard hardness	>98.1	Hardness independent of applied load and microstructure

TABLE 16.7 Details of Common Hardness Tests

Test	*Indenter*	*Description*	*Equation*	*Notes*
Brinell	Hardened steel ball	Brinell hardness number BHN is applied force divided by surface area of indentation	$BHN = F/\pi Dt$	Spherical indenters not used for ceramics
		Meyer hardness number MHN uses projected area	$MHN = 4F/\pi d^2$	
Vickers	Square pyramid	Vickers hardness number (VHN) using contact area	$VHN = 1.854\ F/a^2$	The ceramics community uses mainly the number calculated using the projected area. Need to be careful when comparing data from different sources
		VHN using projected area	$VHN = 2.000\ F/a^2$	
Knoop	Elongated pyramid	Knoop hardness number KHN	$KHN = 14.2\ F/L^2$	
Rockwell	Various indenter types/loads	Dimensionless number and various hardness scales		Widely used for metals, not often for ceramics except cemented carbides

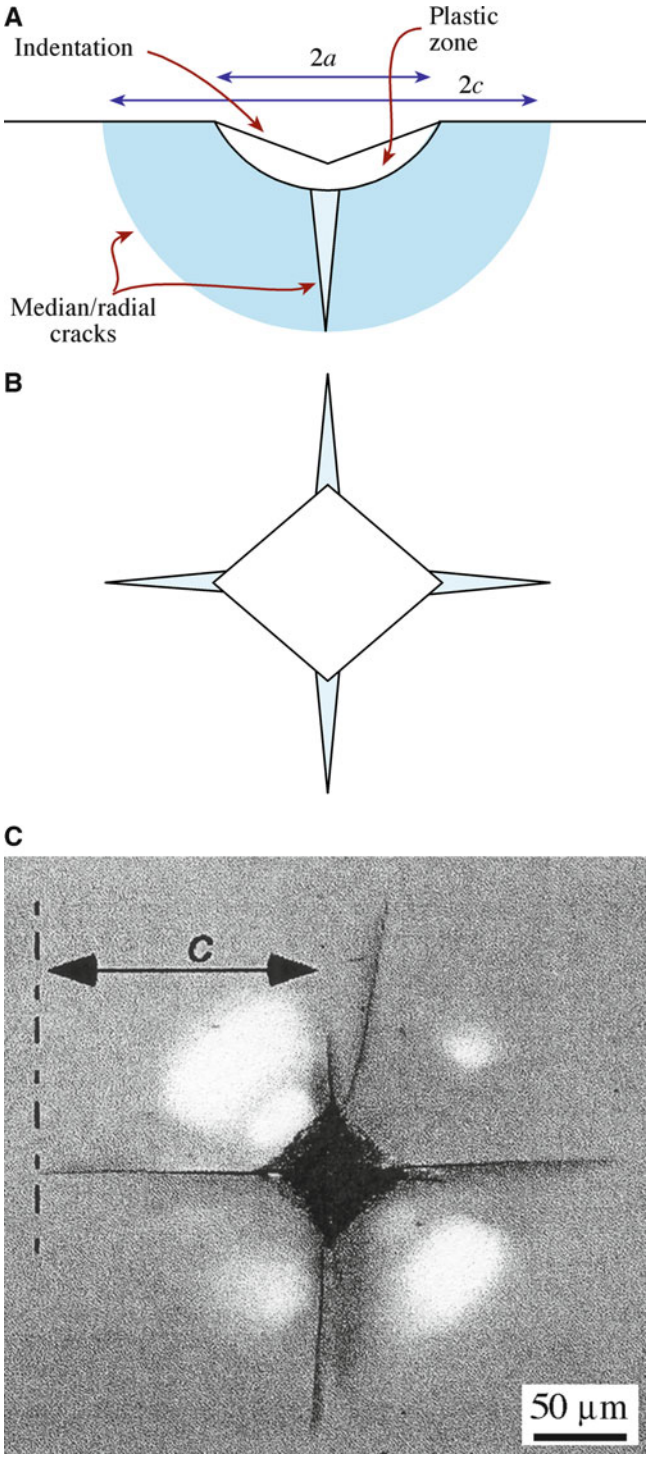

FIGURE 16.17. Cracks at an indent allow determination of K_{IC}.

where α is a numerical factor that depends on the shape of the indenter. For a Vickers indenter, $\alpha = 2$. P is the load in newtons.

The critical stress intensity factor is obtained by assuming that the applied stress intensity caused by the load is equal to the critical stress intensity for crack propagation:

$$K_{Ic} = \frac{\zeta(E/H)^{\frac{1}{2}}P}{c^{\frac{3}{2}}} \tag{16.14}$$

where ζ is a dimensionless constant, which for ceramics has an average value of 0.016 ± 0.004. The use of indentation techniques for determining K_{Ic} has been the subject of many studies since being introduced by Lawn and Wilshaw (1975). The most commonly used variant, termed the indirect method, uses indentation followed by determination of the strength after indentation using bend testing. The main concern is to ensure that the crack does not grow between indentation and bend testing. To minimize effects of reactive species, such as water, a drop of oil may be placed on the indent. Tests seem to give reproducible values for K_{Ic}.

16.12 NANOINDENTATION

The nanoindentation technique was developed in the 1980s because of the need to determine the mechanical properties of thin films and surfaces that had been modified (e.g., by ion implantation). To avoid the influence of the substrate, it is necessary that the penetration depth of the indenter is >10% of the film thickness. Consequently, penetration depths are on the order of nanometers rather than millimeters, which is common for conventional indentation tests.

Nanoindentation is also used to test small volumes of material. The low loads used mean that the extent of cracking is much smaller than with conventional indentation methods.

The two parameters that are often of most interest in nanoindentation testing are:

- Elastic modulus
- Hardness

Load (P) versus depth of penetration (h) curves, also called compliance curves, are the output from a nanoindentation test. The curves are obtained as load is applied to the indenter tip up to some maximum value and then back to zero. Figure 16.18 shows a general compliance curve for a material that undergoes both elastic and plastic deformation. When the load applied to the indenter is released, the material attempts to return to its original shape. The slope of the elastic unloading region (dP/dh) can be used to determine the modulus and hardness. There are several different equations depending on the tip geometry. If the material is plastically deformed, it cannot return to its original shape and there is a residual impression, h_r, as seen in Figure 16.18. The magnitude of h_r is greater for a metal such as steel than for a ceramic such as sapphire.

Nanoindentation is a powerful technique because the shape of the load–displacement curve can be used to

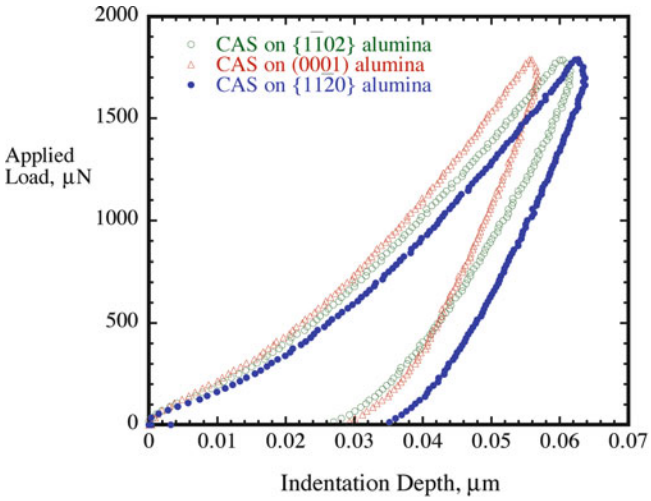

FIGURE 16.18. Load–displacement data on the 1.8 mN indentations of CAS films on three different alumina substrates.

identify effects such as phase transformations, cracking, and film delamination during indentation. It is also important when studying the mechanical properties of nanomaterials, such as carbon nanotubes. There is reference now to a picoindenter, which is a combination of a nanoindenter and an atomic force microscope.

16.13 ULTRASONIC TESTING

The basic principle of ultrasonic testing is that the velocity of an ultrasonic wave through a material is related to its density and elastic properties. This is one example of a dynamic method for determining elastic constants, such as Young's modulus and shear modulus. Dynamic methods are more accurate than static methods, with uncertainties of <0.5% (±10% would be more typical for static methods).

To determine the shear modulus and Poisson's ratio, we need the velocity of the longitudinal and transverse waves, v_L and v_t. The equations are:

$$\mu = \rho v_t^2 \tag{16.15}$$

$$\nu = \frac{1 - 2(v_t/v_L)^2}{2\left[1 - (v_t/v_L)^2\right]} \tag{16.16}$$

$$\mathcal{E} = 2\,\mu(1 + \nu) \tag{16.17}$$

Conversely, if we know the elastic moduli, we can determine the magnitude of the sound velocities. For ceramics with high moduli and low density, the sound velocities are much higher than for many metals. The propagation of sound waves through ceramics is particularly important during earthquakes. The Earth's crust is composed primarily of silica and aluminosilicates. Using equations 16.15 and 16.16, we can show that for SiO_2 (the primary constituent of rocks such as granite) the longitudinal waves are the first shocks to arrive after an earthquake, followed by the transverse waves: $v_L = 6.04$ km/s and $v_t = 4.1$ km/s for quartz. The surface waves are the last to arrive, having a velocity <4 km/s, but they often have the most devastating effect.

Ultrasonic testing is widely used in the concrete industry for determining the presence, or absence, of voids, cracks, and other imperfections and for measuring deterioration that might have occurred due to age or through fire or frost damage.

TRANSVERSE WAVE VELOCITIES

	Al_2O_3	Al
μ	163 GPa	25 GPa
ρ	3,970 kg/m^3	2,710 kg/m^3
v_t	6.4 km/s	3.0 km/s

16.14 DESIGN AND STATISTICS

When we measure the strength of a series of equivalent ceramic specimens, we typically find considerable scatter in the results. The reason is due to the size distribution of flaws that are responsible for failure. This behavior is very different from that of metals. Consequently, we have to adopt different design approaches when we use ceramics.

When we design components using metals, we determine the maximum stress present in the component and then select a metal that has a larger strength. A reasonable safety margin is often included. This approach is referred to as deterministic design. It does not work with ceramics because of the large scatter. Rather, we have to use a probabilistic approach where we represent this scatter in a quantitative way so that these materials can be used safely. The most popular method is to use Weibull statistics, which are based on the weakest link approach. The analogy is to consider a chain the strength of which is determined by the weakest link.

The Weibull distribution function is shown in Figure 16.19 and gives the probability of survival (P_s) or, alternatively, the probability of failure (P_F), of a stressed volume V.

$$P_S = 1 - P_F = \exp\left[-\int_V \left(\frac{(\sigma - \sigma_{min})}{\sigma_0}\right)^m dV\right] \tag{16.18}$$

The Weibull distribution function contains three parameters:

m = Weibull modulus tells us how rapidly the strength falls as we approach σ_0

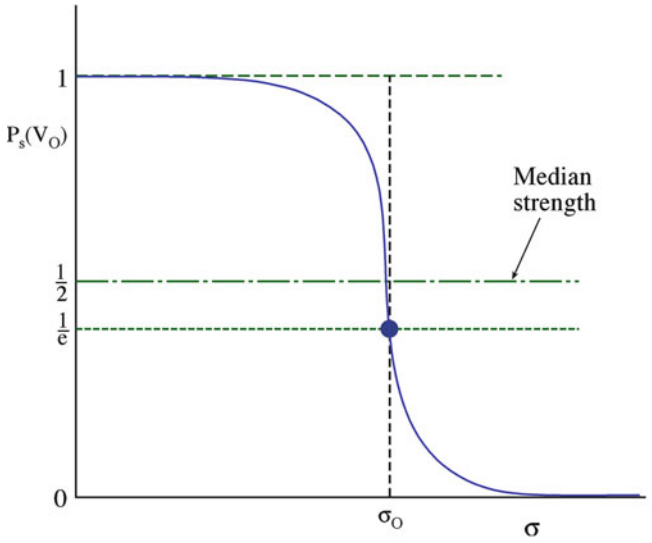

FIGURE 16.19. Weibull distribution function.

σ_0 = characteristic strength for which the survival probability is 0.37 ($1/e$)

σ_{min} = stress level below which the probability of failure is zero.

Because there is always a possibility, albeit slight, of our component having a very large flaw, we usually set $\sigma_{min} = 0$. This leads to the two-parameter form that is used for ceramics.

$$P_S = \exp\left[-\int_V \left(\frac{\sigma}{\sigma_0}\right)^m dV\right] \qquad (16.19)$$

If the full volume is under uniform uniaxial tension, then we can write equation 16.19 as:

$$P_S = \exp\left[-\left(\frac{\sigma}{\sigma_0}\right)^m\right] \qquad (16.20)$$

For other geometries, we need to include the loading factor, L_F. This takes into account the stress distribution. For uniaxial tension $L_F = 1$; for other loading geometries see Table 16.9. The product ($L_F V$) is often termed the effective volume, V_{eff}, as it indicates how "effectively" the body is being stressed.

Taking the natural logarithm of both sides of equation 16.20 we get:

$$\ell n\left(\frac{1}{P_S}\right) = \left(\frac{\sigma}{\sigma_0}\right)^m$$

If we take natural logarithms, again we get

$$\ell n\left[\ell n\left(\frac{1}{P_S}\right)\right] = m\ell n\left(\frac{\sigma}{\sigma_0}\right) = m\ell n\sigma - m\ell n\sigma_0$$

Now, if we plot $-\ln\ln(1/P_S)$ versus $\ln\sigma$, we get a straight line of slope $-m$, as shown in Figure 16.20. The higher the Weibull modulus, the lower is the variability of strength. Values for ceramics are often in the range of 5–20 (compared, for example, to steels, which have values of about 100). Figure 16.21 shows how the Weibull modulus affects the survival probability.

TABLE 16.9 Examples of Loading Factors

Geometry	*Loading factor, L_F*
Uniaxial tension	1
Pure bending	$1/[2(m+1)]$
3-Point bending	$1/[2(m+1)^2]$
4-Point bending	$(mL_i + L_o)/[2L_o(m+1)^2]$

L_i inner span, L_o outer span

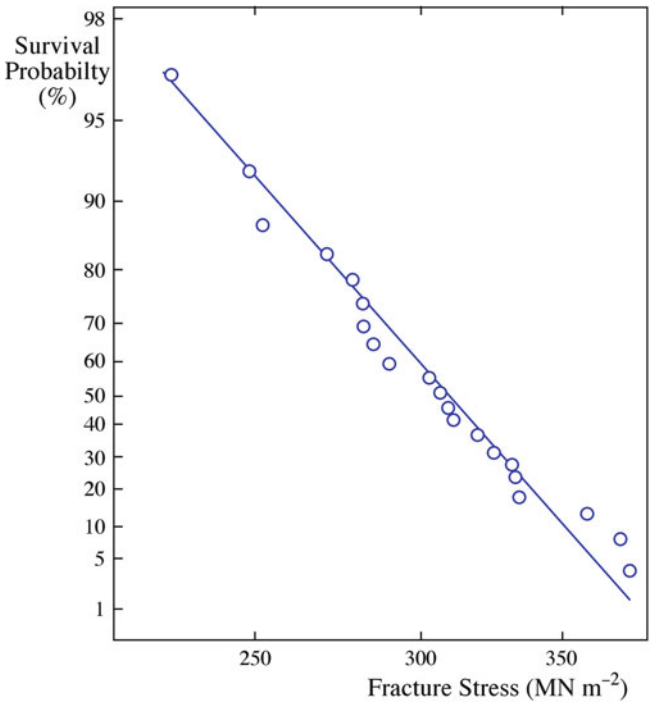

FIGURE 16.20. Weibull plot showing probability of failure as a function of fracture stress.

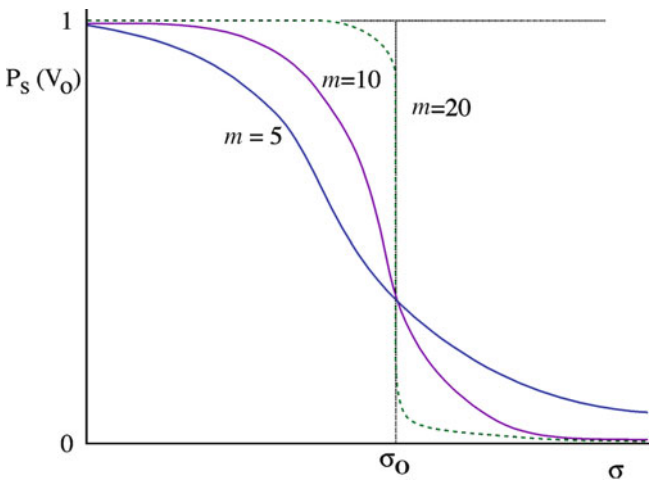

FIGURE 16.21. Effect of m on survival probability. When m changes, P_s changes.

The Weibull modulus, which is the parameter in which we are often most interested, is obtained experimentally by testing a batch of samples. We need a large number of specimens to get an accurate value of m. Usually a minimum of 30 samples is required, and this typically gives m within 20%. Up to 100 samples is not uncommon, and it gives m with >90% confidence.

Sequence of steps to determine m from a set, N, of measured strengths:

1. Rank the specimens in order of increasing strength.
2. Determine P_S. For the jth specimen this is often given as the approximation $P_S(j) = 1 - j/(N+1)$. A more accurate expression that may be used instead is $P_S = 1 - [(j-0.3)/(N+0.4)]$.
3. Plot $-\ln\ln(1/P_S)$ versus $\ln\sigma$ the slope. This can be determined by a least-squares fit and gives m.

In ceramics, there is a volume dependence of the strength. You can illustrate this quite easily using a stick of chalk. As the chalk gets smaller, it gets stronger. The reason is again due to flaws. There is an increased probability of finding a larger flaw in a larger body, as illustrated in Figure 16.22. This effect can be expressed mathematically as

$$P_S = \exp\left[-\left(\frac{V}{V_0}\right)\left(\frac{\sigma}{\sigma_0}\right)^m\right]$$

where $V = nV_0$. An example of the size effect is shown in Figure 16.23 for Si_3N_4 springs. The springs have different diameters of the wire and of the coil, and different numbers of coils were measured.

Complications arise if we have different flaw populations; for example, we may have pores and inclusions introduced during sintering and surface flaws introduced during grinding. The different flaws may lead to different Weibull distributions and different Weibull moduli. Figure 16.24A illustrates superposition of two flaw types and Figure 16.24B for a sample containing surface and volume flaws. Then, we have new equations:

For two different surface flaw types:

$$P_S = \exp\left[-\left(\frac{\sigma_c}{\sigma_1}\right)^{m_1} - \left(\frac{\sigma_c}{\sigma_2}\right)^{m_2}\right]$$

For flaw type 1, we have σ_1 and m_1; for flaw type 2 we have σ_2 and m_2.

For two different types of volume flaws:

$$P_S = \exp\left[-\frac{V_{eff1}}{V_0}\left(\frac{\sigma_c}{\sigma_{v1}}\right)^{m_1} - \frac{V_{eff2}}{V_0}\left(\frac{\sigma_c}{\sigma_{v2}}\right)^{m_2}\right]$$

As you now realize, it is impossible to design a ceramic where the probability of failure is zero. Table 16.10 gives some examples of what might be considered acceptable probabilities of failure.

Proof testing can be used to truncate the extreme tail of the Weibull distribution. Components are tested up to a certain proof-test stress, σ_{PT} (Figure 16.25) for a short period of time. The weakest ones obviously fail and can be weeded out. We then have increased confidence in the remaining components. We often have to proof test to stresses close to the design stress. For a ceramic with $m = 10$, reducing the risk of rupture from 0.10 to 0.05 requires that the component be proof tested to 93% of the design stress. To reduce the probability of failure by an order of magnitude, down to 0.02, the part must be proof tested to 99% of the design stress (Figure 16.26). We have

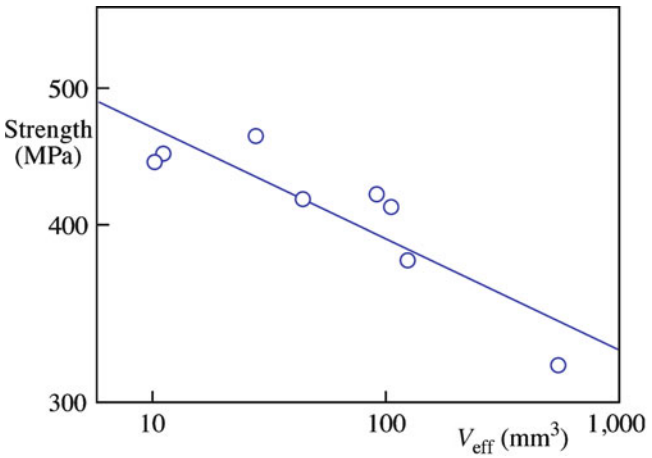

FIGURE 16.23. Fracture stress as a function of volume for Si_3N_4 springs.

STRENGTH & VOLUME

The strength of metal samples does not depend on volume.

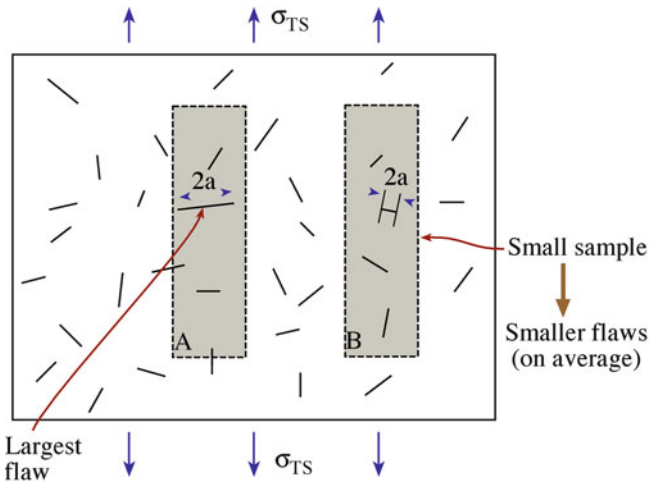

FIGURE 16.22. The largest flaw is the weakest link and the source of failure. Smaller samples have smaller flaws.

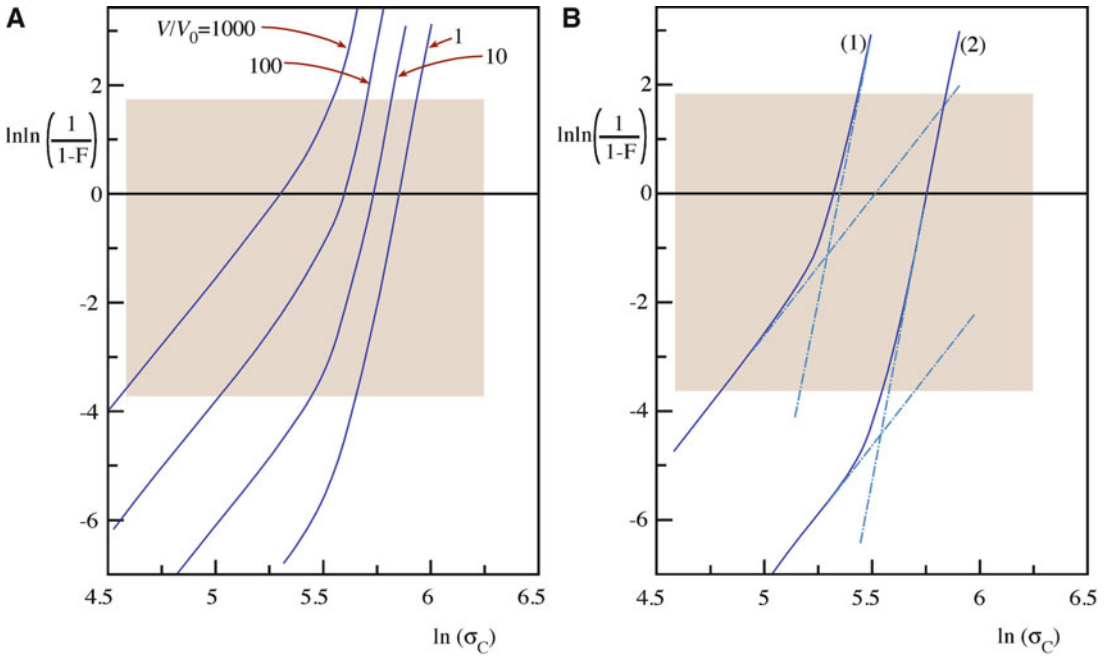

FIGURE 16.24. (A) Different flaws lead to different values of *m*. (B) Weibull plot for a sample having both surface and volume flaws.

TABLE 16.10 Suggested Failure Probabilities

P_F	*Possible consequences of failure*	*Example*
0.3	Slight inconvenience	Sticks of chalk
10^{-2}	Inconvenience and small expense	Ceramic cutting tool
10^{-6}	Injury	Window on a vacuum system
10^{-8}	Loss of life and significant expense	Ceramic protective tile on space shuttle

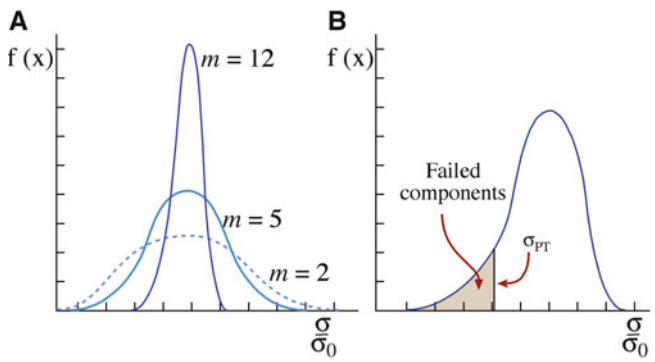

FIGURE 16.25. (A) Probability distributions for different values of *m*. (B) Proof testing up to σ_{PT} removes the weakest components from the distribution.

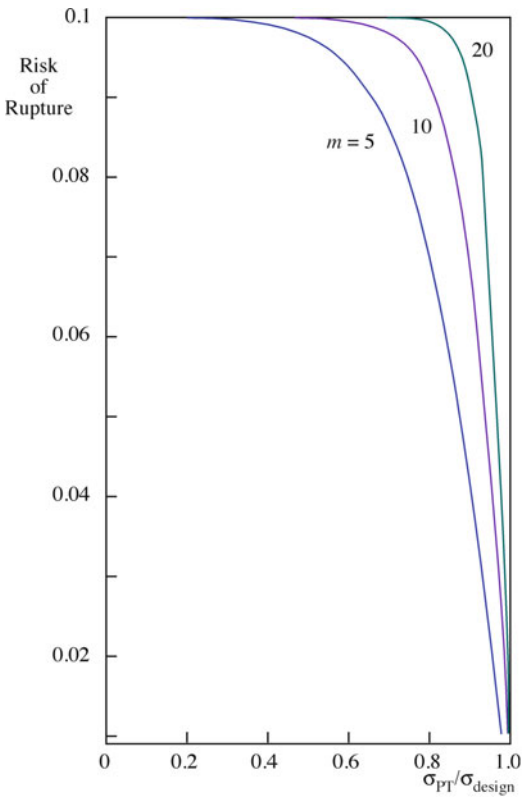

FIGURE 16.26. Plot showing the risk of rupture after proof testing to the ratio of proof test stress to design stress.

a good level of confidence in the remaining components withstanding any stress $<\sigma_{PT}$.

CARES (*C*eramics *A*nalysis and *R*eliability *E*valuation of *S*tructures) is a public-domain program from the National Aeronautics and Space Administration (NASA) that incorporates Weibull statistics. The program was formally known by the less friendly acronym SCARE (*S*tructural *C*eramics *A*nalysis and *R*eliability *E*valuation).

NASA CARES program is available at: http://www.grc.nasa.gov/WWW/LPB/cares/life/refs.html/.

Considerations and assumptions with the use of Weibull statistics:

- We need to ensure that the conditions under which we are testing match those in service. For example, flaws in a component may appear during service as a result of oxidation or corrosion that might not be present in the test sample.
- There is a complex distribution of flaws.
- More than one type of flaw may be present.

16.15 SPT DIAGRAMS

Stress–probability–time diagrams incorporate the time dependence of strength into failure statistics and give lifetime predictions. An illustration of the use of SPT diagrams is in bioceramics.

An important requirement for any implant material is how long it will last. Because of the nature of failure of ceramic components, it is not possible to provide a specific and definite lifetime for each individual implant. Rather, we have to express failure in terms of probabilities. Figure 16.27 is an applied stress versus probability of time to failure (SPT) diagram for medical grade alumina. It shows that for a 30-year survival period, with failure of no more than 1 in 100 components, the maximum tensile stress that can be applied is limited to <200 MPa. If stresses of 250 MPa are applied to the ceramic component, within 3 years 4% of the implants are likely to fail and by 30 years 7% will probably fail. Use of SPT diagrams such as these, together with finite element analysis of local stress distributions, make it possible to design ceramic components that have very low probabilities of failure during the lifetime of the patient. Numerous clinical studies have been performed on patients receiving a total hip prosthesis. One of the main problems that have been encountered is that of wear between the head (ball) and the socket. Although there is considerable variation in the data, it is generally found that the wear rate for systems with metal balls is much higher than that with alumina balls. Also, alumina balls in alumina sockets produce the least wear of any combination of materials, as indicated in Table 16.11.

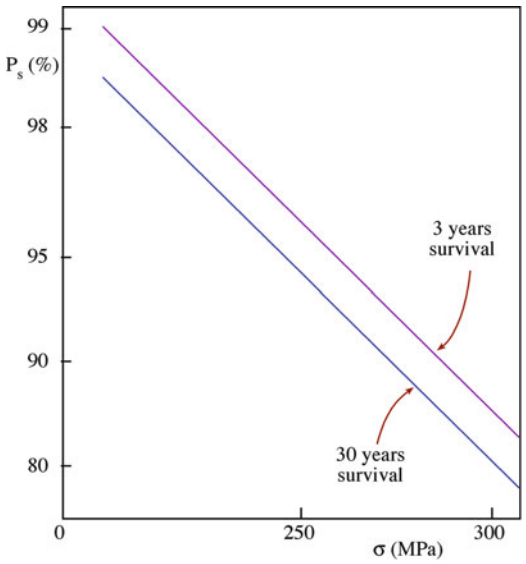

FIGURE 16.27. Stress–probability–time (SPT) diagram for medical-grade Al_2O_3. Survival probability decreases with increasing stress and longer times.

TABLE 16.11 Average Annual Wear Rates of Articulating Surfaces in Total Hip Prosthesis

Materials	*Wear Rate (μm/year)*
Co-Cr-Mo Alloy/UHMWPE	200
Alumina/UHMWPE	20–130
Alumina/alumina	2

CHAPTER SUMMARY

Flaws dominate the mechanical properties of ceramics. They determine how we test them and how we design components from them. Flaws are also the reason why ceramics are stronger in compression than tension. In this chapter, we described the methods used to measure mechanical properties of ceramics. The important ones are bend testing, compression testing, and indentation. To determine the mechanical properties of small volumes we use nanoindentation. This technique is especially important for thin films, surfaces, and nanomaterials. An understanding of statistics is particularly important when using ceramics in load-bearing applications. The Weibull approach is the one most widely used for ceramics.

PEOPLE AND HISTORY

Mohs, Fredrich (1773–1839). A German mineralogist, his original paper on the scratch test and the eponymous hardness scale was published in *Grundriss der Mineralogie* in 1822.

Poisson, Siméon Denis (1781–1840). A French mathematician, he was more suited to mathematics than medicine because of his clumsiness. This was not an impediment for a mathematician! In 1837, he published a

paper on probability, which described the Poisson distribution. During his career, Poisson published more than 300 mathematical works and was reported to have said "Life is good for only two things, discovering mathematics and teaching mathematics."

Ringer, Sidney (1835–1910). A British physician and physiologist, his original salt solution was developed in 1882 and used to prolong the survival time of tissue taken from a frog's heart. The solution used to test biomaterials differs in composition from that developed for amphibians.

Young, Thomas (1773–1829). An English physician physicist, he could read fluently by age two and presented his first paper to the Royal Society at the young age of 20. By 1801, he was a professor at the Royal Institution in London. He was probably best known for his classic double-slit experiment, which demonstrated the wave nature of light.

Weibull, E.H. Waloddi (1887–1979). He was a Swedish engineer. The original paper describing his statistical analysis was published in 1939, "A Statistical Theory of the Strength of Materials" (*Ingeniöersvetenskaps-akademiens Handlingar* 151, 1–45). Weibull was a frequent visitor to Wright Patterson Air Force Base in Ohio and lectured at the Air Force Institute of Technology. In 1972, he was awarded the American Society of Mechanical Engineers gold medal for his achievements. King Carl XVI Gustav of Sweden presented Weibull the Great Gold medal from the Royal Swedish Academy of Engineering Sciences in 1978.

EXERCISES

16.1 In Figure 16.7, the experimental data for the unstabilized samples deviate from the predicted values for Young's modulus. (1) What do we mean by "unstabilized"? (2) How can you account for the difference in the predicted values and experimental values?

16.2 Is Young's modulus affected more by the presence of an intergranular glass phase or an equal amount of porosity? Justify your answer with a suitable calculation.

16.3 Ten rectangular test specimens of MgO were tested in three-point bending. The bars were 1 cm thick and 0.5 cm high and were tested over a 5-cm span. The failure loads for each are given in ascending order: 140, 151, 154, 155, 158, 165, 167, 170, 173, and 180 kg. Calculate the modulus of rupture (MOR) for each sample and the average MOR for this group of samples.

16.4 A commercially available polycrystalline alumina is tested using three different methods: three-point bend, four-point bend, uniaxial tension. The resulting MOR values are 550, 410, and 175 MPa, respectively. What conclusions can you make about the material from these data?

16.5 The soda-lime silicate glass sample shown in Figure 16.17 was indented with a load of 20 N. Estimate the (1) hardness and (2) fracture toughness. (3) How else might you obtain the fracture toughness?

16.6 For the data shown in Figure 16.20, determine the Weibull modulus.

16.7 The following data were obtained in a series of tensile strength tests on polycrystalline silicon carbide specimens (in MPa): 334, 289, 232, 294, 252, 337, 256, 339, 308, 365, 311, 341, 286, 314, 274, 285, 382, 379, 282, 324, 316. (1) Determine the Weibull modulus for these samples. (2) Would you expect the value of m for a set of steel specimens to be higher or lower than the value you calculated in part (1). Assuming that these SiC specimens were made by hot pressing, would you expect m for a series of SiC made by sintering to be higher or lower?

16.8 Calculate using the Voight and Reuss models the bounds for Young's modulus of MgO–Al_2O_3 composites as a function of volume fraction.

16.9 Explain briefly why there is a size dependence for the strength of ceramics but not for metals.

16.10 Sketch stress–strain plots for polycrystalline MgO at (1) 25°C, (2) 1,000°C, (3) 1,700°C, and (4) 2,800°C.

16.11 Explain why the mode I load type is most important for ceramics.

16.12 We haven't listed any values for K_{1c}. Discuss and research some values using the library or other resources and compare them to metals and a polymer such as polymethylmethacrylate (PMMA). (Acknowledge your resources).

16.13 If the fracture toughness of steel is 50,000 psi$\sqrt{\text{in}}$, how does this compare to that of glass and concrete? (We are deliberately using antique units: convert them). How much can the value for glass vary?

16.14 Consider three otherwise dense, small-grain ceramic cubes with the same overall density but with equally spaced spherical pores of diameters 10 nm, 100 nm, and 1 μm, respectively. How will this porosity affect the elastic moduli?

16.15 Mohs hardness is widely used in one field and indentation in another. Discuss the advantages of the former.

16.16 Figure 16.16 stops in the early 1980s. Use library resources to discuss this observation. Discuss the indenter shape that would be suitable for a fiber.

16.17 Figure 16.18 shows three curves. Calculate the different properties of the three orientations.

16.18 Explain why the Voigt and Reuss assumptions lead to equations 16.6 and 16.7, respectively.

16.19 Challenge: relate Figures 16.20 to 16.21.

16.20 Challenge: we refer to the $d^{-1/2}$ dependence in Figure 16.5. How can this be true for both distributions, and what does it tell us?

GENERAL REFERENCES

ASM International (1991) Engineered materials handbook, vol 4, Ceramics and glasses. ASM International, Materials Park, A useful reference

Balluffi RW (2011) Introduction to elasticity theory for crystal defects. Cambridge University Press, Cambridge, Very new—hope to see it soon!

Cook RF, Pharr GM (1994) Mechanical properties of ceramics. In: Cahn RW, Haasen P, Kramer EJ (eds) Materials science and technology. VCH, Weinheim, pp 339–407

Davidge RW (1979) Mechanical behavior of ceramics. Cambridge University Press, Cambridge, UK, A brief introduction

Fischer-Cripps AC (2002) Nanoindentation. Springer, New York

Gordon JE (2006) The new science of strong materials, or why you don't fall through the floor. Princeton University Press, Princeton, revised edn, An excellent introduction to mechanical properties of materials, the original was 1968

Green DJ (1998) An introduction to the mechanical properties of ceramics. Cambridge University Press, Cambridge, UK

Lawn B, Wilshaw TR (1975) Indentation fracture — principles and applications. J Mater Sci 10:1049, The paper that showed how to derive K_{1c} from indenter experiments

McColm IJ (1990) Ceramic hardness. Plenum, New York

Munz D, Fett T (1999) Ceramics: mechanical properties, failure behavior, materials selection. Springer, Berlin

Richerson DW (2006) Modern ceramic engineering, properties, processing and use in design, 3rd edn. Taylor and Francis, Boca Raton, Chapter 18 describes design approaches for ceramics

Sines G, Adams M (1978) Compression testing of ceramics. In: Fracture mechanics of ceramics, vol 3. Plenum, New York, pp 403–434

Wachtman JB, Cannon WR, Matthewson MJ (2009) Mechanical properties of ceramics. Wiley, New York ('revised' Ed).

SPECIFIC REFERENCES

Blum JJ (1975) Slice synthesis of three dimensional work-of-fracture specimens. Eng Fract Mech 7:593, The slice model for determining Y*, the geometric "constant" in K_{Ic} measurements. (c.f., Munz et al)

Hashin Z, Shtrikman S (1963) A variational approach to the theory of the elastic behavior of multiphase materials. J Mech Phys Solids 11:127

Lawn BR, Marshall DB (1979) Hardness, toughness, and brittleness – indentation analysis. J Am Ceram Soc 62:347–350, Defines the brittleness index (BI)

Munz DM, Shannon JL, Bubsey RT (1980) Fracture-toughness calculation from maximum load in 4 point bend tests of Chevron Notch specimens. Int J Fract 16:R137–142, The straight-through crack assumption approach to determination of Y*. the geometric "constant" in K_{Ic} measurements (c.f., Blum et al)

Ridgeway RR, Ballard AH, Bailey BL (1933) Hardness values for electrochemical products. Trans Electrochem Soc 63:267

Syed SA, Wahl KJ, Colton RJ (2000) Quantitative study of nanoscale contact and pre-contact mechanics using force modulation. Mat Res Soc Symp Proc 594:471–476, Developed the picoindenter—a combination of a nanoindenter and an AFM

Thoman DR, Bain LJ, Antle CE (1969) Inferences on the parameters of the Weibull distribution. Technometrics 11:445, Used numerical methods to determine m

Weibull W (1951) A statistical distribution function of wide applicability. J Appl Mech 18:293–297, The original

WWW

Lots at http://www.nist.gov/mml/ceramics/ if you look hard